Asian Journal of Atmospheric Environment
Vol. 9-1, pp. 91-99, March 2015
doi: http://dx.doi.org/10.5572/ajae.2015.9.1.091

ISSN(Online) 2287-1160
ISSN(Print) 1976-6912

Multi-wavelength Raman LIDAR for Use in Determining the Microphysical, Optical, and Radiative Properties of Mixed Aerosols

Kwon-Ho Lee and Young Min Noh[1),*]

Department of Atmospheric & Environmental Sciences, Gangneung-Wonju National University, Gangneung, Korea
[1)]International Environmental Research Centre (IERC), Gwangju Institute of Science & Technology (GIST), Korea

*Corresponding author. Tel: +82-62-715-2470, E-mail: nym@gist.ac.kr

ABSTRACT

The Multi-wavelength Raman LIDAR (MRL) system was developed to enable a better understanding of the complex properties of aerosols in the atmosphere. In this study, the microphysical, optical, and radiative properties of mixed aerosols were retrieved using the discrete aerosol observation products from the MRL. The dust mixing ratio, which is the proportion of dust particles to the total mixed, was derived using the particle depolarization ratio. It was employed in the retrieval of backscattering and extinction coefficient profiles for dust and non-dust particles. The vertical profiles of aerosol optical properties were then used as input parameters in the inversion algorithm for the retrieval of microphysical parameters including the effective radius, refractive index, and the single scattering albedo (SSA). Those products were successfully applied to an analysis of radiative flux using a radiative transfer model. The relationship between the MRL derived extinction and aerosol radiative forcing (ARF) in short-wavelength was assessed over Gwangju, Korea. The results clearly demonstrate that the MRL-derived extinction profiles are a good surrogate for use in the estimation of optical, microphysical, and radiative properties of aerosols. It is considered that the analytical results shown in this study can be used to provide a better understanding of air quality and the variation of local radiative effects due to aerosols.

Key words: Aerosol, Extinction, LIDAR, Retrieval, Radiative effect

1. INTRODUCTION

Atmospheric aerosols are one of the largest sources of air pollution; they can affect global atmospheric chemistry and the Earth's radiation budget, thereby contributing to climate change (Myhre *et al*., 2013). It is known that major aerosol species are inorganic, water-soluble, soot, dust, and sea-salt. Their size distribution can be expressed as a bimodal lognormal function (Hess *et al*., 1998), and in general most aerosols related to pollution such as carbonaceous and sulfate particles are fine particles, whilst dust and sea-salt are coarse. In addition, the size distribution of atmospheric aerosols varies depending on the formation of the aerosols involved, and their dynamic processes (Reid *et al*., 1998).

LIght Detection And Ranging (LIDAR) is a powerful technique that uses a high temporal and spatial resolution to measure the vertical distribution of atmospheric aerosols. LIDAR measures elastic light scattering in relation to molecules and aerosols, and can retrieve aerosol backscatter and extinction profiles using an analytical solution to the LIDAR equation with an initial assumption (Fernald, 1984; Klett, 1981). However, the aerosol extinction coefficients derived from the elastic backscatter signal can be erroneous due to large errors in the use of assumed values, such as the LIDAR ratio (extinction-to-backscatter ratios, hereafter LR).

Only the Raman LIDAR technique allows measurements of reliable aerosol extinction profiles (Ansmann *et al*., 1991), and is able to measure the backscattering and extinction coefficient of aerosols simultaneously. Ansmann *et al*. (1992) developed Raman LIDAR to measure water vapor, carbon dioxide (CO_2), LR, and aerosol extinction profiles. In addition, a number of studies in literature show that the Raman signal is useful in estimating aerosol optical properties and identifying aerosol type (Müller *et al*., 2005, 1999a, b; Mattis *et al*., 2003; Wandinger *et al*., 2002; Veselovskii *et al*., 2002). For the first time in Korea, a multi-wavelength Raman LIDAR (MRL) system was developed by the Advanced Environmental Monitoring Research Center of the Gwangju Institute of Science and Tech-

nology (ADEMRC/GIST) (Hong *et al*., 2004), and since its development LIDAR instruments have been continuously improved and can now be successfully applied to the observation of mixed aerosols in the atmosphere (Shin *et al*., 2014; Tatarov *et al*., 2012; Noh *et al*., 2011, 2007).

The main objectives of this study are: (i) to explore the possibility of establishing the MRL-retrieved aerosol optical and microphysical properties of a mixture of dust and pollution particles; and (ii) to investigate the variations in the radiative processes of these aerosol mixtures in relation to the vertical distribution of aerosol layers. This paper is structured as follows: the instruments used and methods employed are introduced in Section 2. Section 3 then presents the results of MRL measurements. The work is concluded in Section 4, and further suggestions are also presented.

2. INSTRUMENTS AND METHODS

The MRL is multi-wavelength backscatter system that points vertically to the zenith and operates in the coaxial mode. Fig. 1 and Table 1 describe the systematic characteristics of the MRL system. The MRL uses a commercial Nd:YAG laser as light source, and this operates on three wavelengths (λ=355 nm, 532 nm, and 1064 nm) with a fixed repetition rate of 10 Hz; the pulse energy at the three wavelengths is 140 mJ, 154 mJ, and 640 mJ, respectively. The emitted laser pulses have a divergence of less than 0.2 mrad after 5X beam expansion. In addition, a 14 inch Schmidt-Cassegrain telescope (focal length f=3.91 m, field of view=0.4-0.5 mrad) is used to receive the backscattered signal. The MRL currently makes the following measurements: elastic backscatter signals at 355 nm, 532 nm, and 1064 nm; two nitrogen vibration Raman signals at 387 nm and 607 nm; and polarized signals at 532 nm. When making measurements, the incomplete overlap between the outgoing laser beam and the field of view of the telescope is ignored for the backscatter signal because the ratios of the elastic scattering signals and the nitrogen Raman signals are computed (Wandinger and Ansmann, 2002); this allows the MRL to retrieve vertical profiles of the backscatter coefficient (β_p) from 400 m above the ground.

Fig. 2 shows the three-part data analysis used to acquire aerosol products from the MRL. In the first part, the received backscatter signal is used to determine the profiles of aerosol optical properties such as the depolarization ratio, extinction, and backscattering for dusty and non-dusty particles. These products are then used to retrieve the refractive index (denoted as m_r (real part) and m_i (imaginary part)), effective radius

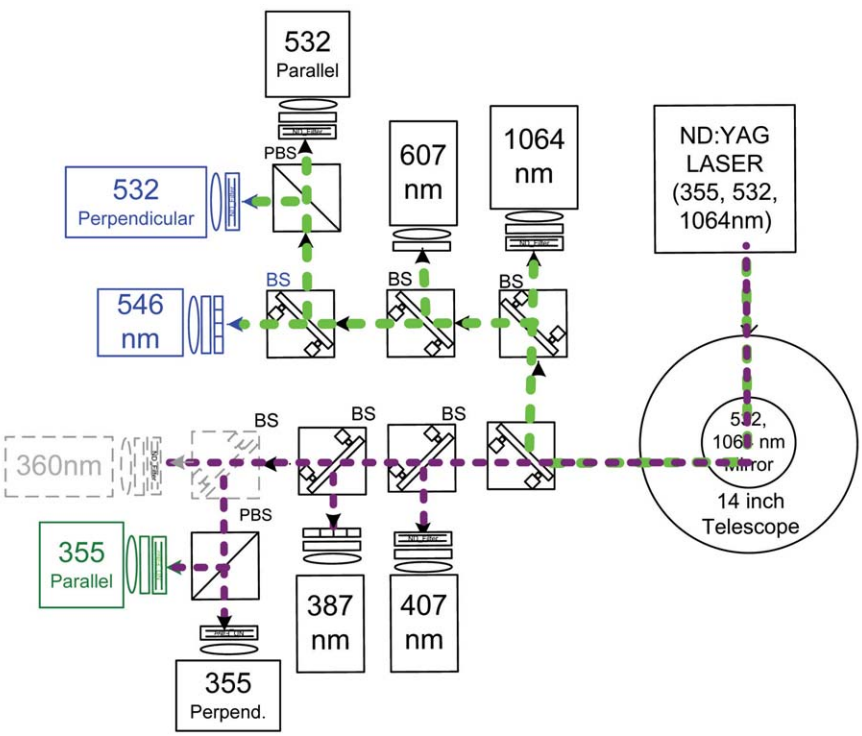

Fig. 1. Systematic diagram of Multi-wavelength Raman LIDAR at GIST. Backscattered signals observed from the telescope are separated by a beam splitter (BS).

Table 1. Specification of multi-wavelength Raman LIDAR of GIST.

Parts	Characteristics
Transmitter	
Laser Type	Nd:YAG
Wavelength (pulse energy)	(355 nm (140 mJ), 532 nm (154 mJ), 1064 nm (640 mJ)
Repetition rate	10 Hz
Beam divergence	0.2 mrad after 5X beam expansion
Pulse duration	< 10 ns
Receiver optics	
Optical design	Schmidt-Cassegrain telescope 14-inch
Focal length	3910 mm
Field-of-view	0.5-0.4 mrad (changeable)
Data acquisition system	
Detector	Photomultiplier tubes (PMT)
Wavelengths (nm)	355, 360, 387, 407, 532 ($=$,$\perp$), 546, 607, and 1064
Bandwidth of interference filter (nm)	5, 3, 0.72, 0.97, 1, 3, 0.45, 1

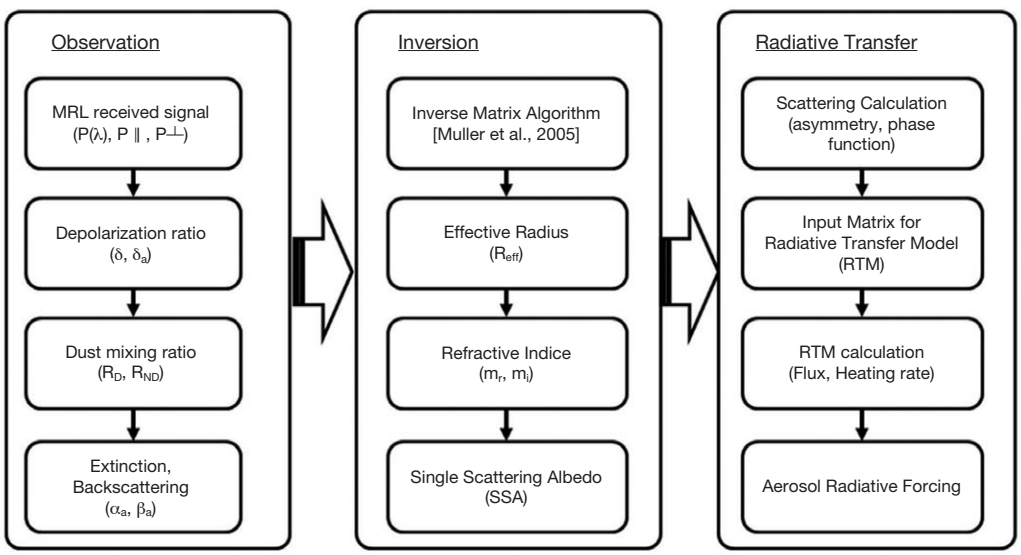

Fig. 2. Schematic workflow diagram of data processing of the multi-wavelength Raman LIDAR receiving signal.

(r_{eff}), and the single scattering albedo (SSA), using a numerical inversion technique based on the inverse matrix method suggested by Müller *et al*. (1999a, b). Those parameters are required to aid in radiative transfer calculations. By definition of scattering theory, the refractive index and single scattering albedo controls light scattering and absorption properties of aerosol particles. Following this, the aerosol optical and microphysical parameters are employed to simulate the atmospheric radiative transfer. In this simulation, the Santa Barbara discrete ordinance radiative transfer (DISORT) atmospheric radiative transfer (SBDART) code (Ricchiazzi *et al*., 1998) was used.

Determination of the vertical profile of the particle backscatter coefficient at 355 nm and 532 nm relies on the LIDAR inversion technique, and this is implemented following reception of the nitrogen vibration Raman signals at 387 nm and 607 nm, as proposed by Ansmann *et al*. (1990). The LIDAR equation used for Raman backscatter signal is expressed as:

$$P_{\lambda R}(z)=K_{\lambda R}\frac{O(z)}{z^2}N_R(z)\frac{d\sigma_{\lambda R}(\pi)}{d\Omega} \times \exp\left\{-\int_0^z\left[\alpha_{\lambda 0}^{aer}(\xi)+\alpha_{\lambda 0}^{mol}(\xi)+\alpha_{\lambda R}^{aer}(\xi)+\alpha_{\lambda R}^{aer}(\xi)\right]\right\} \quad (1)$$

where $P_{\lambda R}(z)$ are the return signals from distance z at the Raman wavelength of $_{\lambda R}$; $O(z)$ is the overlap correction factor; $K_{\lambda R}$ is the depth-independent system parameters; $N_R(z)$ is the molecule number density of the Raman-active gas; and $d\sigma_{\lambda r}(\pi)/d\Omega$ is the range-independent differential Raman cross section for the

backward direction. Using the reference signal, the particle extinction coefficient (α_{aer} or α_p) can be determined as:

$$\alpha_{aer}(z)=\frac{\frac{d}{dz}\left\{\ln\left[\frac{N_{ref}(z)}{P_{ref}(z)\cdot z^2}\right]\right\}-\alpha_{\lambda}^{mol}(z)-\alpha_{\lambda_{ref}}^{mol}(z)}{1+\left(\frac{\lambda}{\lambda_{ref}}\right)^{k}} \quad (2)$$

where $N_{ref}(z)$ is the molecular number density of the reference gas, and $k=1$, except for ice clouds. The backscattering coefficient (β_{aer} or β_p) can be derived as:

$$\beta_{aer}(z)=[\beta_{aer}(z_0)+\beta_{mol}(z_0)]\times\frac{P_{\lambda ref}(z_0)P_{\lambda}(z)}{P_{\lambda}(z_0)P_{\lambda ref}(z)}\frac{N_{ref}(z)}{N_{ref}(z_0)} \times\frac{\exp\left\{-\int_{z0}^{z}\left[\alpha_{\lambda ref}^{aer}(\xi)+\alpha_{\lambda ref}^{mol}(\xi)\right]\right\}}{\exp\left\{-\int_{z0}^{z}\left[\alpha_{\lambda}^{aer}(\xi)+\alpha_{\lambda}^{mol}(\xi)\right]\right\}}-\beta_{mol}(z) \quad (3)$$

where z_0 is reference height with $\beta_{mol}(z_0)\gg\beta_{aer}(z_0)$. Using α_p and β_p determined by Eqs. (2) and (3), LR is then determined as:

$$LR(z)=\frac{\alpha_{aer}(z)}{\beta_{aer}(z)} \quad (4)$$

The advantage of the Raman LIDAR technique is that it can measure extinction and backscattering directly, eliminating the need for an assumption of the extinction-to-backscatter ratios when solving the LIDAR equation. However, the only disadvantage of using the Raman LIDAR technique is the relatively weak Raman scattering compared to the Rayleigh or fluorescence scattering, but this limitation can be overcome by the use of high power lasers and/or long integration times. Thus aerosol optical property profiles can be resolved in both time and space, enabling a vertical snapshot for the precise identification of aerosol distribution. In this respect, many studies have successfully demonstrated the capabilities of MRL for use in the monitoring of aerosols (i.e. Tatarov *et al.*, 2012; Müller *et al.*, 2010; Noh *et al.*, 2009).

The MRL can retrieve aerosols optical properties such as the particle backscatter coefficients at 355 nm, 532 nm, and 1064 nm; the particle extinction coefficients at 355 nm and 532 nm; the linear particle depolarization ratio at 532 nm; the water-vapor mixing-ratio; and profiles of silicon-dioxide (SiO_2). The available aerosol products relating to MRF retrieval are listed in Table 2. Note that profiles of the silicon-dioxide (quartz) signal are tracers of the mineral dust concentration, and for this contribution we use the signals required for measuring particle backscatter and extinction coefficients at 355 nm and 532 nm, and the linear depolarization ratio (aerosols+molecules) (denoted as δ). The particle depolarization ratio (δ_p) used in this study is defined as:

$$\delta_p=\frac{\delta(z)R(z)-\delta_m}{R(z)-1} \quad (5)$$

where δ_m denotes the molecular depolarization ratio; and $R(z)$ is the scattering ratio. The dust mixing ratio (R_D) is then the ratio between dust backscattering to total backscattering coefficient, and can be mathematically expressed by δ_p for dust particles (δ_D) and for non-dust particles (δ_{ND}), and in this respect we used the values of 0.35 and 0.02, which were recommend-

Table 2. List of optical, microphysical, and radiative properties of aerosol inferred from the multi-wavelength Raman LIDAR.

Category	Products
Extensive optical particle parameter	Particle volume backscatter coefficient at 355 nm, 532 nm, and 1064 nm Particle volume extinction coefficient at 355 nm and 532 nm Raman quartz backscatter coefficient at 360 nm and 546 nm
Intensive optical particle parameter	Linear aerosol depolarization ratio at 532 nm Particle LIDAR ratio at 355 nm and 532 nm Extinction-related Ångström exponent 355/532 nm pair Backscatter-related Ångström exponent 355/532 nm pair and 532/1064 nm pair Raman-quartz backscatter-related Ångström exponent 360/546 nm pair
Microphysical parameter (from inversion of extensive optical properties)	Real and imaginary part of the complex refractive index Number, volume, and surface-area concentration Particle volume size distribution Particle effective radius
"High-end" particle parameters	Single-scattering albedo Mineral quartz concentration
Application	Upward/Downward Flux Heating Rate Aerosol Radiative Forcing

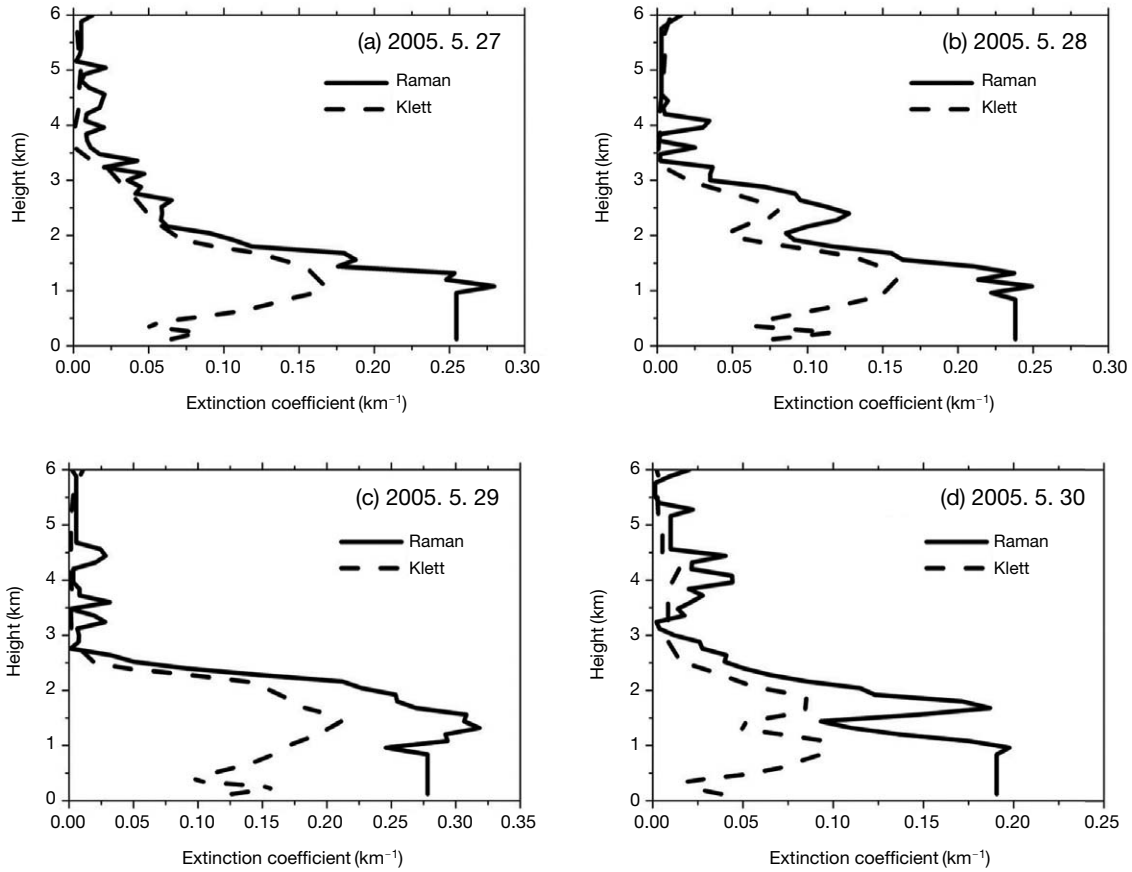

Fig. 3. Aerosol extinction coefficient profiles derived using the Raman method (solid line) and the Klett method (dashed line) during May 27-30, 2005. For the Klett method, a fixed LIDAR ratio of 50 was used for the extinction coefficient retrieval.

ed in previous studies (Noh *et al*., 2008, 2007).

$$R_D = \frac{(\delta_P - \delta_{ND})(1+\delta_D)}{(\delta_D - \delta_{ND})(1+\delta_P)} \quad (6)$$

3. PROFILING OF AEROSOL OPTICAL /MICROPHYSICAL PARAMETERS

In this study, the MRL system was operated to measure aerosol backscattering, extinction coefficients, the depolarization ratio, and the LIDAR ratio of aerosol at GIST (35.10°N, 126.53°E). Fig. 3 shows an example of aerosol extinction coefficient profiles measured from May 27 to 30, 2005, which were retrieved using the Raman (solid line) and Klett (dashed line) methods, respectively. The shapes of the two curves of the aerosol extinction coefficients are reasonably similar over 3 km, where aerosol loadings barely existed. The extinction coefficients using the Klett method (hereafter, α_p^K) are smaller than those using the Raman method (hereafter, α_p^R) with a mean difference of about $0.04 \pm 0.06\ \mathrm{km}^{-1}$. In addition, its variation trend with height using the Klett method is relatively sharp due to the dependence on aerosol backscatter. In addition, the maximum value of the aerosol extinction coefficient is relatively different. For a single aerosol layer case on May 27, 2005, the maximum value of α_p^R at height of near 1 km was about two times larger than that of α_p^K. Furthermore, multi-layered aerosol signals were found on May 30, 2005.

In Fig. 3, the maximum value of α_p^R at the peaks of layers located at around 1 and 2 km in height are also larger than that by α_p^K. Because we assumed a fixed LR value of 50 for the Klett method, the retrieved value of α_p^K is somewhat different from that of real aerosol particles in the atmosphere. However, aerosol extinction using the Raman method is known to be relatively more accurate than that using the Klett method (Ansmann *et al*., 1992). Therefore, this comparison clearly shows differences in the results of these two retrieval methods in relation to aerosol extinction. In this respect, LR retrieved using the Raman method for

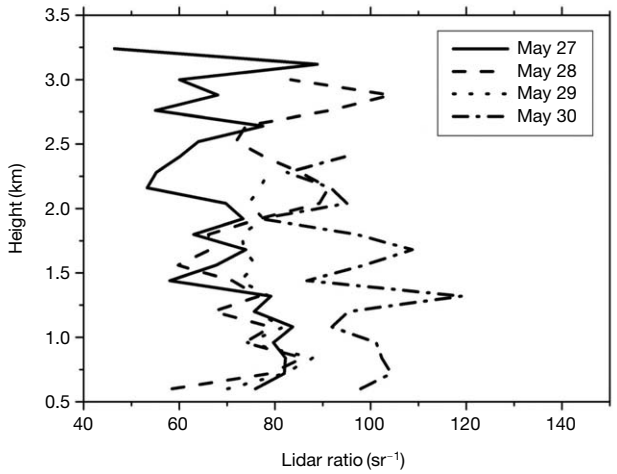

Fig. 4. LIDAR ratio profile measured by the MRL observation during May 27-30, 2005.

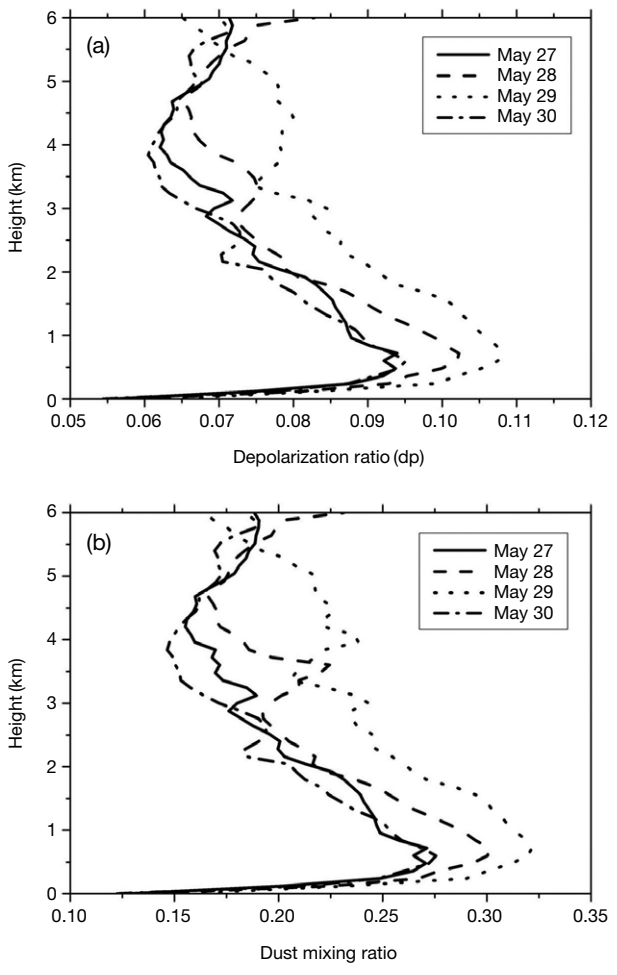

Fig. 5. Depolarization ratio and dust mixing ratio derived from multi-wavelength Raman LIDAR observation during May 27-30 2005.

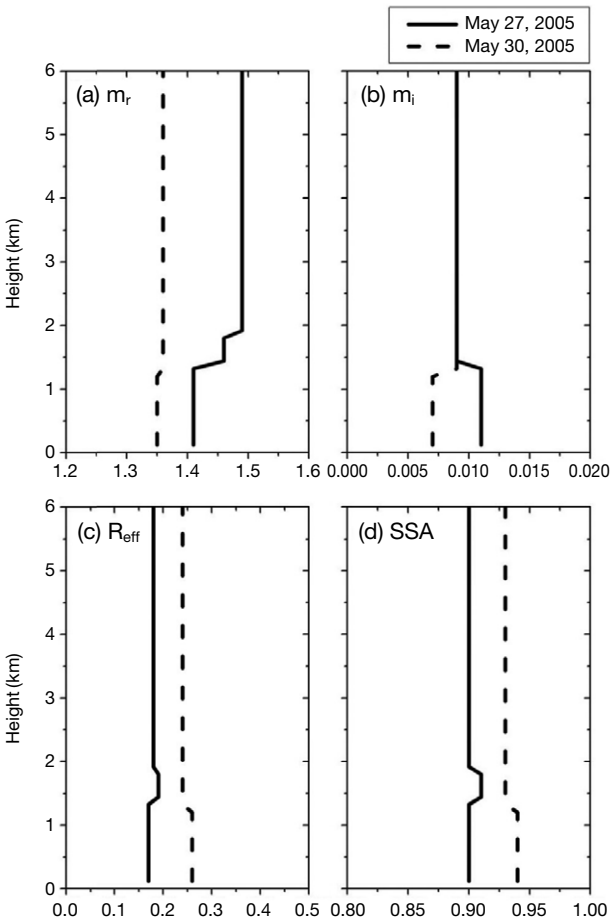

Fig. 6. The multi-wavelength Raman LIDAR inversion products of refractive index, effective radius, and single scattering albedo on May 27 (solid line) and May 30 (dashed line) 2005.

the same days is shown in Fig. 4, where LR profiles from the Raman method range from 45-90 sr^{-1} on May 27, 2005 and 75-120 sr^{-1} on May 30, 2005. As discussed earlier, in Noh *et al*. (2008) these higher values are mainly caused by light-absorbing particles in the atmosphere.

Fig. 5 shows the vertical profiles of daily mean dp at 532 nm and the dust mixing ratio. The particle depolarization ratios are generally higher than 0.06. The larger values of dp are proof of an increase in non-spherical particles at a given height. Maximum dp values were between 0.095 and 0.109 during the observation period. In terms of our observation record, those ranges are close to those of the non-dust regime, because typical dp values range from 0.03 for non-dust to 0.34 for severe dust (Noh *et al*., 2008). The dust mixing ratios in Fig. 5b also confirm that observed backscatter signals consist mainly of non-dust particles (Rd $<$ 0.32).

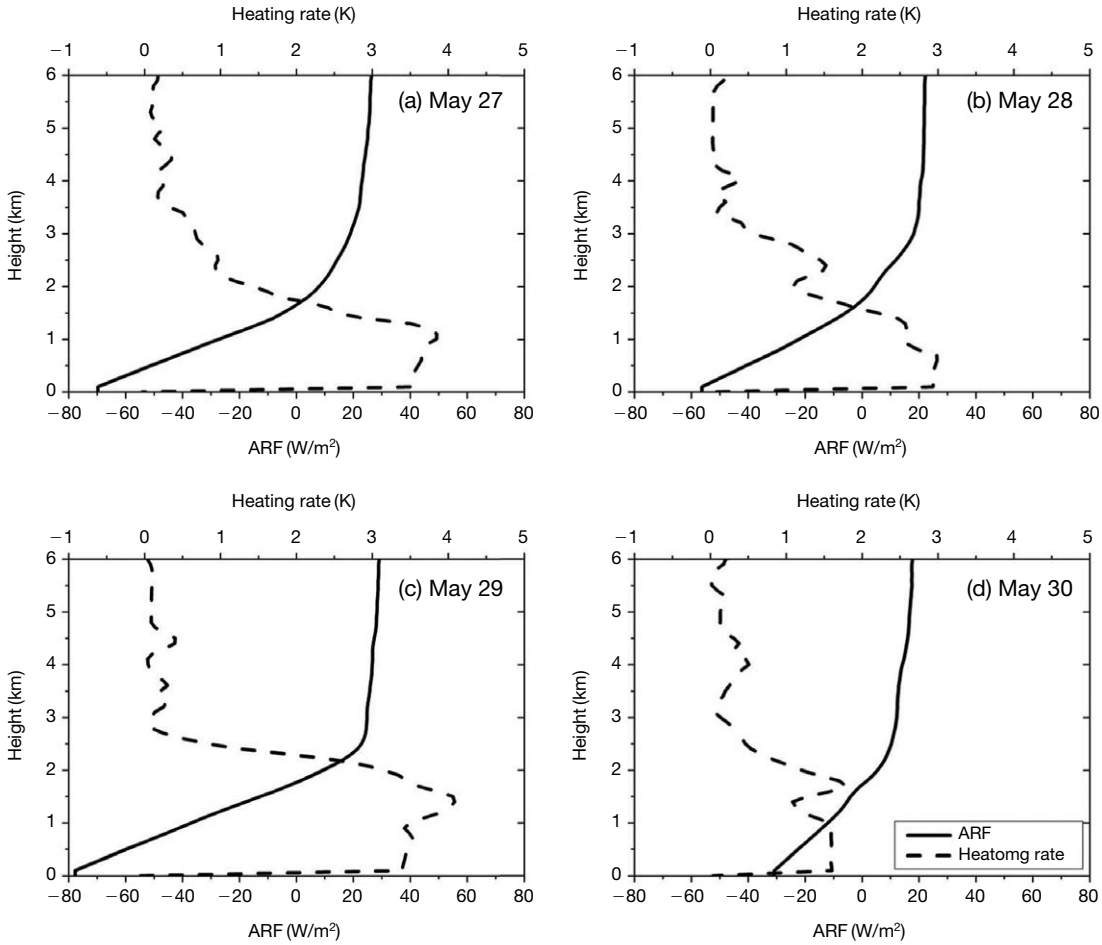

Fig. 7. Aerosol radiative forcing (ARF) (solid line) and heating rate (dashed line) by vertically resolved aerosol properties derived from the multi-wavelength Raman LIDAR.

In Fig. 6, the refractive index, reff, and SSA values from MRL's inversion algorithm are presented for the same days. The mixed aerosol layers under a height of 2 km show little difference in the characteristics of inversion products for both cases. The aerosol layer has a larger refractive index and smaller reff values on May 27, 2005 than on May 27, 2005; the SSA on May 27, 2007 varies from 0.90 to 0.92 whereas the values on May 30, 2005 are at around 0.93. All the above results suggest that particles at different heights have different optical and microphysical properties.

4. AEROSOL RADIATIVE PROPERTIES

After processing data from the MRL observations, the aerosol vertical profiles were used to derive incoming and outgoing shortwave radiation; these profiles included the extinction coefficient, refractive index, r_{eff}, and SSA. Downward ($F_{\downarrow}$) and upward flux ($F_{\uparrow}$) were calculated at each height using aerosol profiles with a standard model atmosphere. The difference in the net flux with and without aerosols is defined as aerosol radiative forcing (ARF), which is a measure of the impact of aerosols on the climate system:

$$ARF=(F_{\downarrow}-F_{\uparrow})_{Aerosol}-(F_{\downarrow}-F_{\uparrow})_{Clean} \quad (6)$$

Using a qualitative set of aerosol observational data from MRL as the input to RTM, we derived the observation-based estimate of ARF at a local atmosphere. Fig. 7 shows the instantaneous ARF estimated for the two case studies. In general, the magnitude of surface level ARF is very large at 80 W/m^2 and -30 W/m^2, respectively. Because these aerosols can absorb radiation, the atmospheric heating rates are increased, and as shown in Fig. 7 the largest heating rates are found to be 3.9 K and 1.7 K. These results imply that the strongest cooling occurs at the surface, and that the strong

warming occurs in the atmosphere because of absorbing aerosol loading (e.g., Li *et al*., 2010; Lee *et al*., 2007). In addition, a large amount of incoming solar radiation is trapped inside the aerosol layer, and this is a significant source of heating to the atmosphere. It is well known that ARF can substantially alter atmospheric stability and influence the dynamic system (Li *et al*., 2010; Niu *et al*., 2010).

5. CONCLUSIONS

The MRL is able to estimate vertically inhomogeneous aerosol loadings with their optical and microphysical properties. A recently developed radiative property calculation coupled with a multi-wavelength inversion technique is able to deliver ARF and atmospheric heating rate profile data. Integrated data processing of MRL measured data and RTM modeled data was performed in Gwangju, Korea. From the case study, the aerosol layers with different vertical profiles of extinction coefficients, LR, refractive index, r_{eff}, and SSA were characterized, with accompanying increases in the extinction coefficients but different absorbing levels. The drop in ARF associated with increased aerosol loadings is explained by the fact that aerosol particles under 2 km can result in the reflection of incoming solar radiation and atmospheric heating by light absorption.

Finally, we conclude that the MRL-derived products and the methods presented here are useful in understanding both the vertical structure and the radiative process relating to aerosols, and as such are useful for performing estimations of local-scale air quality and the climate system.

ACKNOWLEDGEMENT

This work was supported by the Korea Meteorological Administration Research and Development Program under Grant CATER 2012-7080.

REFERENCES

Ansmann, A., Riebesell, M., Wandinger, U., Weitkamp, C., Michaelis, W. (1991) In optical remote sensing of the atmosphere, Optical Society of America, Summaries of papers presented at the Optical Remote Sensing of the Atmosphere Topical Meeting, Williamsburg, VA, pp. 206-208.

Ansmann, A., Riebesell, M., Weitkamp, C. (1990) Measurement of atmospheric aerosol extinction profiles with a Raman lidar. Optics Letters 15, 746-748.

Ansmann, A., Wandinger, U., Riebesell, M., Weitkamp, C., Michaelis, W. (1992) Independent measurement of extinction and backscatter profiles in cirrus clouds by using a combined Raman elastic-backscatter lidar. Applied Optics 31, 7113-7131.

Fernald, F.G. (1984) Analysis of atmospheric lidar observations: some comments. Applied Optics 23, 652-653.

Hess, M., Koepke, P., Schult, I. (1998) Optical properties of aerosols and clouds: The software package OPAC. Bulletin of the American Meteorological Society 79, 831-844.

Hong, C.S., Lee, K.H., Kim, Y.J., Iwasaka, Y. (2004) Lidar measurements of the vertical aerosol profile and optical depth during the ACE-Asia 2001 IOP at Gosan, Jeju Island, Korea. Environmental Monitoring and Assessment 92, 43-57.

Klett, J.D. (1981) Stable analytical inversion solution for processing lidar returns. Applied Optics 20(2), 211-220.

Lee, K.H., Li, Z., Wong, M.S., Xin, J., Wang, Y., Hao, W.-M., Zhao, F. (2007) Aerosol single-scattering albedo estimated across China from a combination of ground and satellite measurements. Journal of Geophysical Research: Atmospheres 112, D22S15, doi:10.1029/2007JD009077.

Li, Z., Lee, K.-H., Wang, Y., Xin, J., Hao, W.-M. (2010) First observation-based estimates of cloud-free aerosol radiative forcing across China. Journal of Geophysical Research: Atmospheres 115 (D00K18), doi:10.1029/2009JD013306.

Mattis, I., Ansmann, A., Wandinger, U., Müller, D. (2003) Unexpectedly high aerosol load in the free troposphere over central Europe in spring/summer 2003. Geophysical Research Letters 30, 2178, doi:10.1029/2003GL018442.

Müller, D., Ansmann, A., Freudenthaler, V., Kandler, K., Toledano, C., Hiebsch, A., Gasteiger, J., Esselborn, M., Tesche, M., Heese, B., Althausen, D., Weinzierl, B., Petzold, A., Von Hoyningen-Huene, W. (2010) Mineral dust observed with AERONET Sun photometer, Raman lidar, and in situ instruments during SAMUM 2006: shape-dependent particle properties. Journal of Geophysical Research: Atmospheres 115, D11207.

Müller, D., Mattis, I., Wandinger, U., Ansmann, A., Althausen, D., Stohl, A. (2005) Raman lidar observations of aged Siberian and Canadian forest fire smoke in the free troposphere over Germany in 2003: Microphysical particle characterization. Journal of Geophysical Research: Atmospheres 110, D17201.

Müller, D., Wandinger, U., Ansmann, A. (1999a) Microphysical particle parameters from extinction and backscatter lidar data by inversion with regularization: theory. Applied Optics 38, 2346-2357.

Müller, D., Wandinger, U., Ansmann, A. (1999b) Microphysical particle parameters from extinction and backscatter lidar data by inversion with regularization: simulation. Applied Optics 38, 2358-2368.

Myhre, G., Shindell, D., Bréon, F.-M., Collins, W., Fuglestvedt, J., Huang, J., Koch, D., Lamarque, J.-F., Lee,

D., Mendoza, B., Nakajima, T., Robock, A., Stephens, G., Takemura, T., Zhang, H. (2013) Anthropogenic and Natural Radiative Forcing. In: Climate Change 2013: The Physical Science Basis. Contribution of Working Group I to the Fifth Assessment Report of the Intergovernmental Panel on Climate Change [Stocker, T.F., D. Qin, G.-K. Plattner, M. Tignor, S.K. Allen, J. Boschung, A. Nauels, Y. Xia, V. Bex and P.M. Midgley (eds.)]. Cambridge University Press, Cambridge, United Kingdom and New York, NY, USA.

Niu, F., Li, Z., Li, C., Lee, K.-H., Wang, M. (2010) Increase of wintertime fog in China: Potential impacts of weakening of the Eastern Asian monsoon circulation and increasing aerosol loading. Journal of Geophysical Research: Atmospheres 115, D00K20, doi:10.1029/2009JD013484.

Noh, Y.M., Kim, Y.J., Choi, B.C., Murayama, T. (2007) Aerosol lidar ratio characteristics measured by a multiwavelength Raman lidar system at Anmyeon Island, Korea. Atmospheric Research 86, 76-87.

Noh, Y.M., Kim, Y.J., Müller, D. (2008) Seasonal characteristics of lidar ratio measured with a Raman lidar at Gwangju, Korea in spring and autumn. Atmospheric Environment 42, 2208-2224.

Noh, Y.M., Müller, D., Mattis, I., Lee, H., Kim, Y.J. (2011) Vertically resolved light-absorption characteristics and the influence of relative humidity on particle properties: Multiwavelength Raman lidar observations of East Asian aerosol types over Korea. Journal of Geophysical Research: Atmospheres (1984-2012), 116, doi:10.1029/2010JD014873.

Noh, Y.M., Müller, D., Shin, D.H., Lee, H.L., Jung, J.S., Lee, K.H. (2009) Optical and microphysical properties of severe haze and smoke aerosol measured by integrated remote sensing techniques in Gwangju, Korea. Atmospheric Environment 43, 879-888.

Reid, J.S., Hobbs, P.V., Ferek, R.J., Blake, D.R., Martins, J.V., Dunlap, M.R., Liousse, C. (1998) Physical, chemical, and optical properties of regional hazes dominated by smoke in Brazil. Journal of Geophysical Research: Atmospheres 103, 32059-32080.

Ricchiazzi, P., Yang, S., Gautier, C., Sowle, D. (1998) SBDART: a research and teaching software tool for plane-parallel radiative transfer in the Earth's atmosphere. Bulletin of the American Meteorological Society 79, 2101-2114.

Shin, S., Noh, Y.M., Lee, K., Lee, H., Müller, D., Kim, Y.J., Kim, K., Shin, D. (2014) Retrieval of the single scattering albedo of Asian dust mixed with pollutants using lidar observations. Advances in Atmospheric Sciences 31(6), 1417-1426, doi: 10.1007/s00376-014-3244-y.

Tatarov, B., Müller, D., Noh, Y.-M., Lee, K.-H., Shin, D.-H., Shin, S.-K., Sugimoto, N., Seifert, P., Kim, Y.-J. (2012) Record heavy mineral dust outbreaks over Korea in 2010: Two cases observed with multiwavelength aerosol/depolarization/ Raman-quartz lidar. Geophysical Research Letters 39, L14801, doi:10.1029/2012GL051972.

Veselovskii, I., Kolgotin, A., Griaznov, V., Müller, D., Wandinger, U., Whiteman, D.N. (2002) Inversion with regularization for the retrieval of tropospheric aerosol parameters from multiwavelidar sounding. Applied Optics 41, 3685-3699.

Wandinger, U., Ansmann, A. (2002) Experimental determination of the lidar overlap profile with Raman lidar. Applied Optics 41(3), 511-514.

Wandinger, U., Müller, D., Bockmann, C., Althausen, D., Matthias, V., Bosenberg, J., Weiβ, V., Fiebig, M., Wendisch, M., Stohl, A., Ansmann, A. (2002) Optical and microphysical characterization of biomass-burning and industrial-pollution aerosols from multiwavelength lidar and aircraft measurements. Journal of Geophysical Research: Atmospheres 107(D21), 8125.

(Received 3 February 2015, revised 11 February 2015, accepted 13 February 2015)